Shock Waves (2012) 22:435–449
DOI 10.1007/s00193-012-0392-9

ORIGINAL ARTICLE

Analytical and numerical investigations of the reflection of asymmetric nonstationary shock waves

Y. Yang · C. Wang · Z. Jiang

Received: 4 January 2012 / Revised: 19 May 2012 / Accepted: 16 June 2012 / Published online: 5 July 2012

Abstract The reflection of asymmetric nonstationary shock waves is analytically and numerically studied in this paper. An analytical approach, which is a combination of the shock dynamic and shock polar methods, is advanced to predict the reflection wave configurations. The numerical simulations are performed by the finite volume method based on the second-order MUSCL-Hancock scheme and the HLLC approximate Riemann solver, with the self-adaptive unstructured mesh. It is found that the transition between the overall regular reflection and overall Mach reflection in the asymmetric nonstationary reflection agrees with the detachment criterion, which is analogous to the reflection in pseudo-steady flows (i.e. shock reflection over a wedge). Some special reflection wave configurations, which have never been observed in steady or nonstationary shock reflections so far, are found to exist in this asymmetric reflection. Furthermore, the domains and boundaries of various overall reflection wave configurations are analytically predicted, and the effect of mis-synchronization is also discussed.

Keywords Asymmetric shock waves · Mach reflection · Detachment criterion

1 Introduction

Nonstationary shock wave reflection over a wedge is often referred to as the reflection in pseudo-steady flows, for the reflection is self-similar and could be transformed into a frame of reference in which the flow is steady. The configurations of this reflection are investigated thoroughly in the past 100 years (e.g. Mach [1]; von Neumann [2,3]; Smith [4]; White [5]; Henderson and Lozzi [6]; Hornung and Taylor [7]; Mirels [8]; Takayama and Ben-Dor [9]; Colella and Henderson [10]; Ben-Dor et al. [11–16]) and several types of wave configurations are observed: regular reflection (RR), von Neumann reflection (vNR), single-Mach reflection (SMR), transitional-Mach reflection (TMR), double-Mach reflection (DMR) and so on.

When two nonstationary shock waves with the same shock Mach number collide with each other, they would be reflected symmetrically (as shown in Fig. 1a). In this situation, the plane of symmetry is equivalent to the wedge surface in the pseudo-steady reflection. However, if the incident shock wave Mach numbers are different, the reflection wave configurations become asymmetrical and thus get more complex (as shown in Fig.1b).

In asymmetric shock wave reflections, many investigations have dealt with the reflections in steady flows. Chpoun and Lengrand [17] initiated the study on asymmetric reflection in steady flows. Their experimental results revealed that, similar to the reflection of symmetric shock waves, a hysteresis in the transition between RR and Mach reflection (MR) also exists in the reflection of asymmetric shock waves. Later, Li et al. [18] conducted the same investigation analytically and experimentally. With the aid of shock polars the hysteresis process was analyzed and the inverse-Mach reflection (InMR) wave configuration was suggested to exist. The domains and transition boundaries of various asymmetric reflection wave configurations in steady flows were predicted. Recently, Hu et al. [19] studied the asymmetric reflection in steady flows analytically and numerically and found that the RR → MR transition can occur between the sonic and maximum-deflection conditions.

Communicated by B. W. Skews.

Y. Yang (✉) · C. Wang · Z. Jiang
State Key Laboratory of High-Temperature Gas Dynamics,
Institute of Mechanics, Chinese Academy of Sciences,
Beijing 100190, China
e-mail: yy@imech.ac.cn

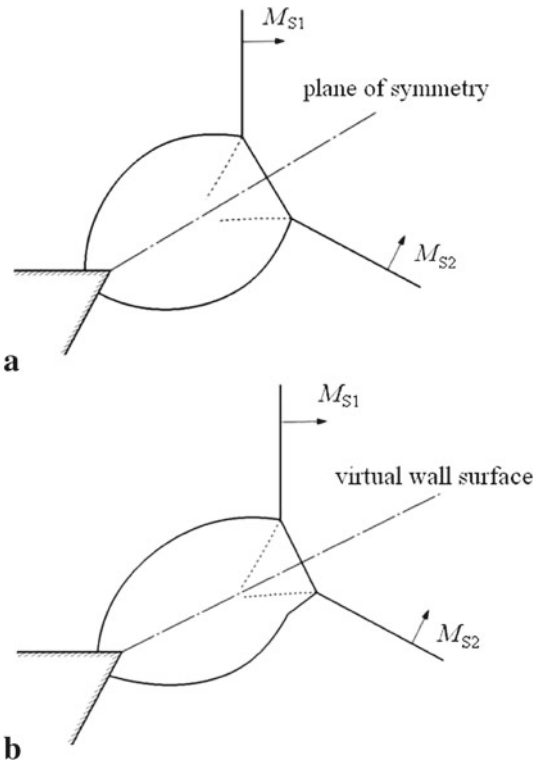

Fig. 1 The reflection of nonstationary shock waves: **a** symmetric reflection; and **b** asymmetric reflection

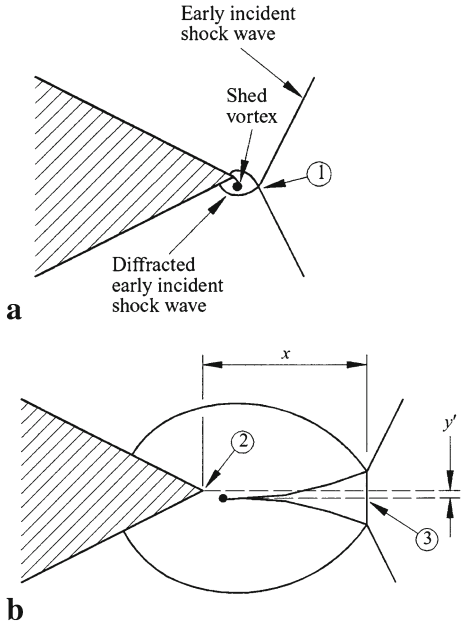

Fig. 2 The schematic of the mis-synchronized case of symmetric reflection of nonstationary shock waves [19]: **a** initial interaction; and **b** interaction at a later stage

For the nonstationary reflection of two interacting shock waves, Barbosa and Skews [20] conducted a series of experiments in a bifurcated shock tube in which a shock wave is split into two plane shock waves of equal strengths that then reflect off each other at the trailing edge of wedge. This nearly symmetric reflection is used to investigate the persistence of regular reflection in pseudo-steady flows. However, it is almost impossible to construct exactly symmetric wave configurations in experiments, so the effect of mis-synchronization is also discussed. For the cases in which two incident shock waves arrive at the trailing edge at slightly different times, it shows that although an asymmetric shock–vortex interaction would occur at the early stage (shown in Fig. 2a), almost the same reflection wave configuration would be generated as the ideal synchronized case at a later time (shown in Fig. 2b), only with a slight displacement of the reflection pattern downwards by a distance y'. Furthermore, Barbosa and Skews [21] also studied the shock–vortex interaction generated in the bifurcated shock tube experimentally and numerically. The detailed shock–vortex interaction wave configuration is described and the generating and developing process of the configuration is recorded. For the reflection of asymmetric nonstationary shock waves, Xie et al. [22] advanced an approach to analyze the wave configuration by the method of shock dynamics. In their studies, a virtual wall surface is assumed to exist and two incident shock waves of different strengths are assumed to be reflected over it. By solving the shock dynamic equations on both sides, the unknown parameters in the flowfield could be obtained. Nevertheless, this analysis can only be applied to the oMR cases, yet cannot predict whether an oMR or an oRR would appear when the overall reflection type is completely unknown.

Compared to the reflection of asymmetric shock waves in steady flows, the shock polar analysis of the reflection of asymmetric nonstationary shock waves is more difficult. In the asymmetric steady shock reflection, for a given flow Mach number M_0 and a constant wedge angle θ_1, the I- and R_1-polars would be fixed when the angle of the other wedge θ_2 changes; while in the asymmetric nonstationary shock reflection, the oncoming flow Mach number, which is obtained by the Galilean transformation, depends partly on the triple point trajectory angle. If one of the incident shock wave Mach number changes, the triple point trajectory angles and hence the oncoming flow Mach numbers, in addition to the location of the virtual wall surface, would all alter with it. Thus, all the I-, R_1- and R_2-polars would shift on the shock polar combination. Furthermore, unlike only SMR and RR existing in steady flows, more different types of MRs are involved in the nonstationary shock reflection.

The reflection of asymmetric nonstationary shock waves is not only a theoretical problem, but also of some application backgrounds, e.g., the interaction of shock waves generated by two adjacent supersonic vehicles or the interaction of two explosive waves. In the present paper, a detailed analytical investigation on the reflection of asymmetric nonstationary

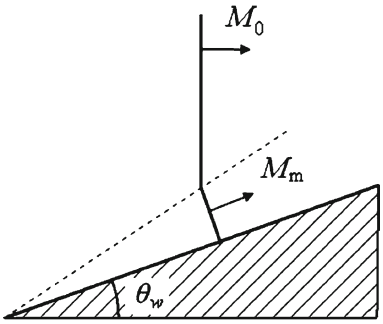

Fig. 3 The nonstationary shock wave reflection over a wedge

shock waves is conducted and scores of numerical simulations, which are provided to verify the analytical results, are also performed.

2 The analysis methods

2.1 Shock dynamic analysis

The shock dynamic theory is a very powerful and relatively easy tool for analyzing the interaction, refraction and reflection of shock waves. In the theory, all the wave structures except the incident shock wave and Mach stem are neglected and the parameters in the flowfield could be obtained by solving the equation based on the geometrical relations. For the reflection of shock wave over a wedge (shown in Fig. 3), the relation between the wedge angle and the Mach numbers of incident shock wave and Mach stem could be expressed as:

$$\tan\theta_w = \left(\frac{M_m}{M_0}\right)\frac{\left[1-\left(\frac{M_0}{M_m}\right)^2\right]^{\frac{1}{2}}\left\{1-\left[\frac{f(M_m)}{f(M_0)}\right]^2\right\}^{\frac{1}{2}}}{1+\frac{f(M_m)}{f(M_0)}\frac{M_m}{M_0}} \tag{1}$$

where

$$f(M) = \exp\left[-\int \frac{2M\mathrm{d}M}{(M^2-1)K(M)}\right] \tag{2}$$

where $K(M)$ is a complicated mathematical function which yields values between 0.3941 and 0.5 for the perfect gas of air.

Figure 4a, b presents the schematic illustrations of the reflections of asymmetric nonstationary shock waves. Similar to shock reflection over a wedge, both the oMR and oRR wave configurations could be formed in the reflection. Xie et al. [22] assumed that there is a virtual wall surface between the incident shock waves for the oMR cases. On each side of the virtual wall surface (1) could be applied, respectively:

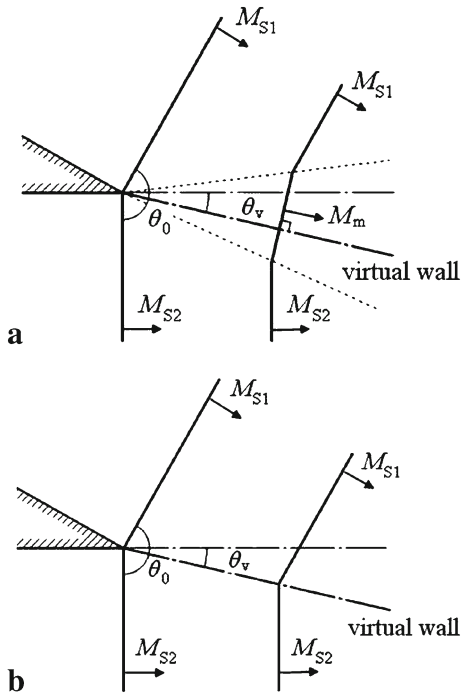

Fig. 4 The reflection of asymmetric nonstationary shock waves: **a** overall Mach reflection; and **b** overall regular reflection

$$\tan\theta_v = \left(\frac{M_m}{M_{S2}}\right)\frac{\left[1-\left(\frac{M_{S2}}{M_m}\right)^2\right]^{\frac{1}{2}}\left\{1-\left[\frac{f(M_m)}{f(M_{S2})}\right]^2\right\}^{\frac{1}{2}}}{1+\frac{f(M_m)}{f(M_{S2})}\frac{M_m}{M_{S2}}} \tag{3}$$

$$\tan(\pi-\theta_0-\theta_v) = \left(\frac{M_m}{M_{S1}}\right)\frac{\left[1-\left(\frac{M_{S1}}{M_m}\right)^2\right]^{\frac{1}{2}}\left\{1-\left[\frac{f(M_m)}{f(M_{S1})}\right]^2\right\}^{\frac{1}{2}}}{1+\frac{f(M_m)}{f(M_{S1})}\frac{M_m}{M_{S1}}} \tag{4}$$

where θ_v denotes the angle between the horizontal line and the virtual wall and θ_0 is the angle between the two incident shock waves. The above set of two equations contains two unknown parameters: θ_v and M_m. Thus, the set is closed and the location of the virtual wall could be solved. For the oRR wave configuration, as shown in Fig. 4b, the virtual wall is also assumed to exist and the location could be derived by the geometrical relations easily:

$$\theta_v = \frac{\pi}{2} - \arctan\frac{M_{S2}\sin\theta_0}{M_{S1}+M_{S2}\cos\theta_0} \tag{5}$$

2.2 Shock polar analysis

The use of shock polar is very convenient for analyzing and understanding shock wave reflection phenomena. For the nonstationary shock wave reflection, it is known that the flowfield should be transformed into a frame of reference attached to the reflection point (RR) or triple point

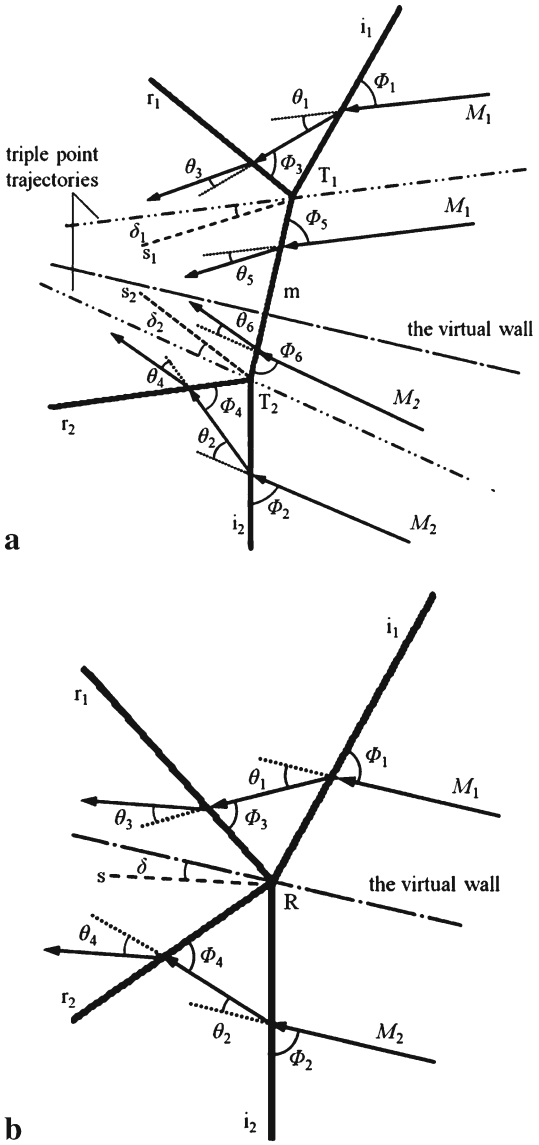

Fig. 5 Schematic illustrations of the flow fields after the Galilean transformations: **a** overall Mach reflection; and **b** overall regular reflection

(MR) before shock polar analysis is performed. Figure 5a, b shows the flowfields of the asymmetric nonstationary reflections after the Galilean transformations. For the oMR wave configuration (shown in Fig. 5a), the triple points (T_1 and T_2) on each side of the virtual wall should be fixed, respectively, by the transformations and then the shock polar could be plotted. The configuration consists of two incident shock waves (i_1 and i_2), two reflected shock waves (r_1 and r_2), a Mach stem (m) and two slipstream lines (s_1 and s_2). The boundary conditions for an oMR are:

$$\theta_1 - \theta_3 = \theta_5 = \delta_1 \tag{6}$$

and

$$\theta_2 - \theta_4 = \theta_6 = \delta_2. \tag{7}$$

In addition, since no obvious wave structures appear behind the Mach stem, the pressure on each side of the virtual wall should also be equal:

$$p_3 = p_5 = p_6 = p_4. \tag{8}$$

When the reflection is symmetric, $\theta_1 = \theta_2$, $\theta_3 = \theta_4$, $\theta_5 = \theta_6$ and $\delta_1 = \delta_2$.

For the oRR wave configuration (shown in Fig. 5b), the reflection point R should be transformed to be stationary and then shock polar analysis could be performed. Two incident shock waves (i_1 and i_2), two reflected shock waves (r_1 and r_2) and a slipstream line are contained in the configuration. The boundary conditions for an oRR are:

$$\theta_1 - \theta_3 = \theta_2 - \theta_4 = \delta \tag{9}$$

and

$$p_3 = p_4. \tag{10}$$

When the reflection is symmetric, $\theta_1 = \theta_2$, $\theta_3 = \theta_4$ and $\delta = 0$.

Figure 6a–i is the schematic shock polar combination of the asymmetric nonstationary reflections, from which it is obvious that there are several different types of wave configurations for different initial conditions. Figure 6a–c shows the cases in which the R_1-polar does not intersect the R_2-polar at all. In these situations, only oMR wave configurations are possible in the flowfields. The oMR wave configuration, which consists of two MRs, has three possibilities depending on the locations of intersections of the R_1- and R_2-polars with the I-polar: two direct-Mach reflections (DiMR) (shown in Fig. 6a), a DiMR and a stationary-Mach reflection (StMR) (shown in Fig. 6b), or a DiMR and an InMR (shown in Fig. 6c). Figure 6d shows the situation in which the R_1-polar is tangent to the R_2-polar. It is the extreme situation in which the oRR wave configuration becomes theoretically possible. Thus, this situation is regarded as the detachment criterion for the reflection of asymmetric nonstationary shock waves. Figure 6e–g shows the cases in which both the oRR and oMR wave configurations are theoretically possible. Similar to shock wave reflection in pseudo-steady flows, the situations are also referred to as the reflections in the dual solution domain. In these situations, the oMR wave configuration may also be three different MR combinations: DiMR+DiMR (shown in Fig. 6e), DiMR+StMR (shown in Fig. 6f) and DiMR+InMR (shown in Fig. 6g). Figure 6h shows the limiting situation in which the oMR wave configuration remains possible. In this shock polar combination, the R_1-polar intersects the R_2-polar exactly at the point located on the I-polar. The situation is regarded as the von Neumann criterion for the asymmetric nonstationary shock wave reflection. The shock polar solution of the oRR wave configuration is presented in Fig. 6i. In this situation, although the R_1- and R_2-polar still intersect the I-polar,

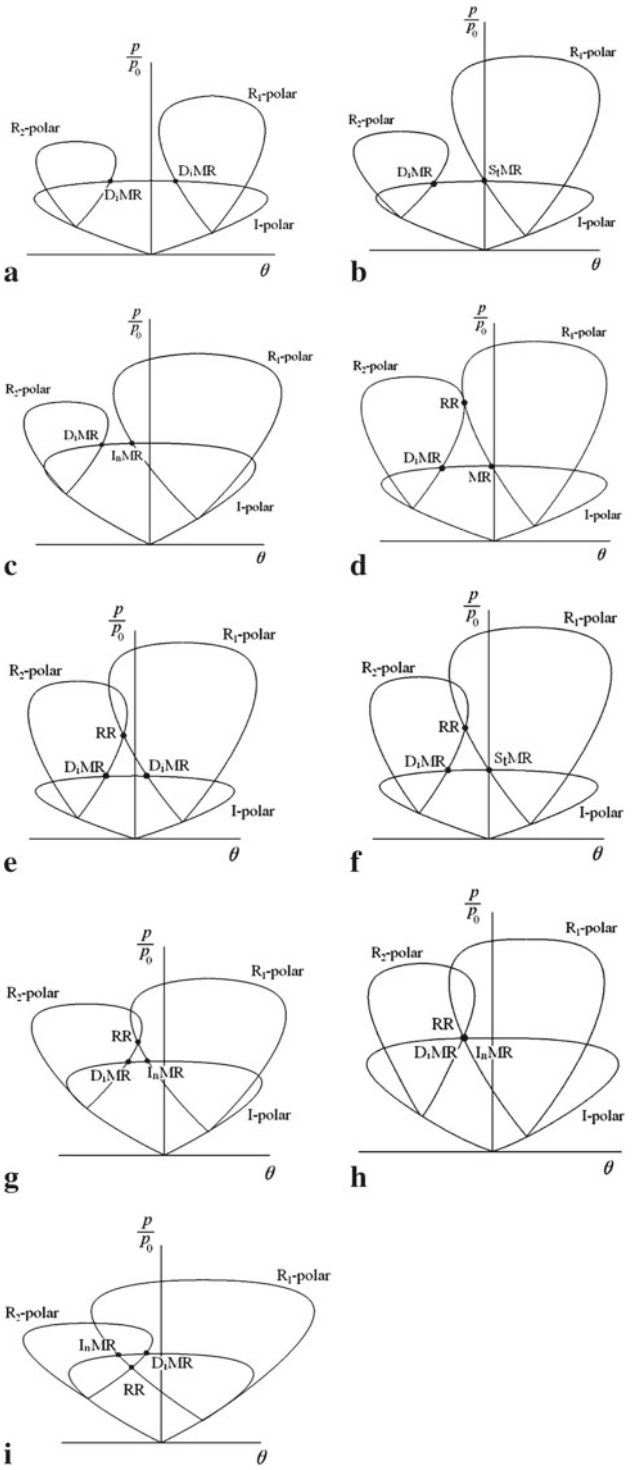

Fig. 6 The schematic shock polar combinations for different overall wave configurations: **a** oMR (DiMR+DiMR); **b** oMR (DiMR+StMR) **c** oMR (DiMR+InMR); **d** detachment criterion; **e** oRR or oMR (DiMR+DiMR); **f** oRR or oMR (DiMR+StMR); **g** oRR or oMR (DiMR+InMR); **h** von Neumann criterion; **i** oRR;

respectively, which indicates that an oMR wave configuration consisting of two MRs could be obtained, the oMR wave configuration would never occur. It is because a diverging stream tube would be formed if this oMR wave configuration appears, and such a stream tube cannot exist in this self-similar nonstationary shock wave reflection. It should be noted that since the oncoming flow Mach numbers with respect to the triple points on the two sides are different in every oMR case, there should be two different I-polars in the accurate shock polar combination, while here only one is plotted just for the purpose of schematic illustration.

2.3 Analytical procedure

Since it is quite difficult and complicated to solve the asymmetric nonstationary shock wave reflection by any approach independently, in this paper, both the shock dynamic and the shock polar methods are used in the course of the investigation. The analytical procedure of the study could be summarized as follows:

1. Assume that the reflection is an oRR configuration, then find the location of the virtual wall by (5).
2. Do the Galilean transformation and then perform the shock polar analysis in the frame of reference attached to the reflection point.
3. If the shock polar combination indicates that an oRR occurs, it implies that the assumption is appropriate and the flow parameters could be obtained from the shock polar solution; if the shock polar combination suggests that the solution lies in the dual solution domain, it needs a further numerical simulation to confirm the wave configuration type; if the shock polar combination indicates that an oRR is impossible to occur, it implies that the assumption is inappropriate and the following procedure should be proceeded:
4. Find the location of the virtual wall by solving the set of (3) and (4). Regard the reflection on each side of the virtual wall as the shock reflection over the virtual wall, then the MR type could be obtained by the domain of various types of reflections in pseudo-steady flows. Figure out the triple point trajectory angle on each side.
5. Do the Galilean transformation on each side and perform the shock polar analyses in the frames of reference attached to the triple points, respectively. Then the flow parameters could be obtained from the shock polar combination.

3 The numerical methods

It is assumed that viscosity effects on nonstationary shock wave reflection are negligible, so the governing equations are simplified to be two-dimensional Euler equations, which can be written as:

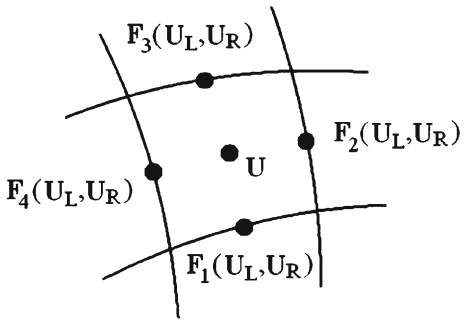

Fig. 7 The governing unit

$$\frac{\partial \mathbf{U}}{\partial t}+\frac{\partial \mathbf{F}}{\partial x}+\frac{\partial \mathbf{G}}{\partial y}=0 \tag{11}$$

where **U**, **F** and **G** denote the state variables and fluxes in x- and y-directions, respectively:

$$\mathbf{U}=\begin{pmatrix}\rho\\ \rho u\\ \rho v\\ e\end{pmatrix},\quad \mathbf{F}=\begin{pmatrix}\rho u\\ \rho u^2+p\\ \rho uv\\ (e+p)u\end{pmatrix},\quad \mathbf{G}=\begin{pmatrix}\rho v\\ \rho uv\\ \rho v^2+p\\ (e+p)v\end{pmatrix} \tag{12}$$

The equation of state for the perfect gas is given by:

$$e=\frac{p}{\gamma-1}+\frac{1}{2}\rho(u^2+v^2) \tag{13}$$

here, the specific heat ratio is taken as 1.4.

In the present numerical simulation, the finite volume method is employed. The governing equations can be converted to the integral form over the governing volume:

$$\int_{\Omega}\frac{\partial \mathbf{U}}{\partial t}\mathrm{d}x\mathrm{d}y+\int_{\Gamma}(\mathbf{F}\mathrm{d}y+\mathbf{G}\mathrm{d}x)=0 \tag{14}$$

where Ω and Γ denote the area and boundary of the governing volume, respectively. Quadrilateral unit is adopted as the governing volume on the unstructured mesh and governing variables are fixed at the center of the unit, as shown in Fig. 7. The HLLC approximate Riemann solver [23] is used to compute the numerical fluxes F($\mathbf{U}_L$, $\mathbf{U}_R$) on the governing unit boundaries and the second-order MUSCL scheme is used for the reconstruction of $\mathbf{U}_L$ and $\mathbf{U}_R$. Moreover, the second-order MUSCL-Hancock scheme is applied for the discretization of time-term [24]. Consequently, the numerical code is second-order both in space and time.

The unstructured mesh is refined according to the density gradient of the flow field and the maximum level of refinement is five. The refinement is controlled by a threshold function which was originally proposed in [25]. If the function value exceeds the refinement threshold value, the governing unit is split into four subunits; if the function value is less than the coarsening threshold value, the four subunits are reunited

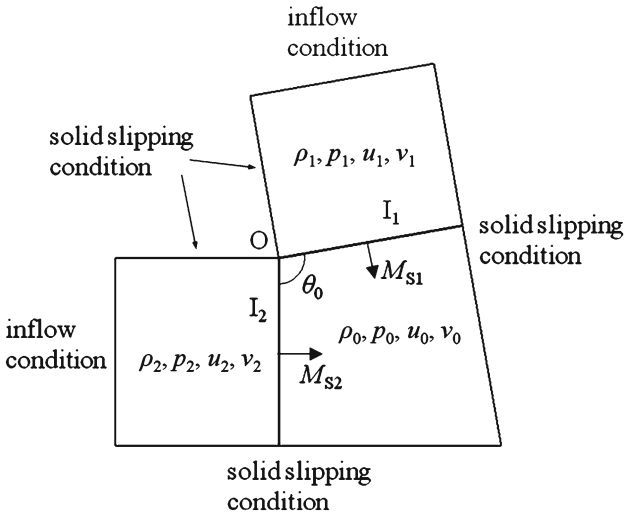

Fig. 8 The computational model

to be one. The threshold function is given by:

$$\varepsilon=\max\left(\frac{|\nabla_l\rho|_c-|\nabla_l\rho|_i}{\alpha_f\rho_c/dl+|\nabla_l\rho|_i},\frac{|\nabla_l\rho|_c-|\nabla_l\rho|_j}{\alpha_f\rho_c/dl+|\nabla_l\rho|_j}\right) \tag{15}$$

where i and j denote two neighboring governing units, and c denotes the midpoint of the boundary between these two units. ∇_l and dl are the gradient and spatial interval from the center of unit i to the center of unit j. α_f is a parameter with a small value to avoid division by zero.

Figure 8 shows the computational model in this study. Region 0 denotes the stationary air ahead of the incident shock waves; regions 1 and 2 denote the air states behind the incident shock waves, which are calculated by the Rankine–Hugoniot relations for the given shock Mach numbers M_{S1} and M_{S2}. The angle between the incident shock waves is θ_0 and the boundary conditions are all marked in the figure. In most parts of the present paper, the model in which the incident shock waves arrive at the wedge apex O at exactly the same time is employed. However, for the purpose of extending the analysis to more general cases, the effect of mis-synchronization is also discussed in the subsequent part of this study.

4 Results and discussion

4.1 The overall Mach and regular reflections

Figure 9a shows the shock polar combination for the reflection of incident shock waves $M_{S1}=4.0$, $M_{S2}=3.8$ and the intersecting angle $\theta_0=100°$. This case corresponds to the first type of reflections illustrated in Fig. 6. As can be seen the R_1- and R_2-polars do not intersect each other, which suggests that only oMR wave configuration is theoretically

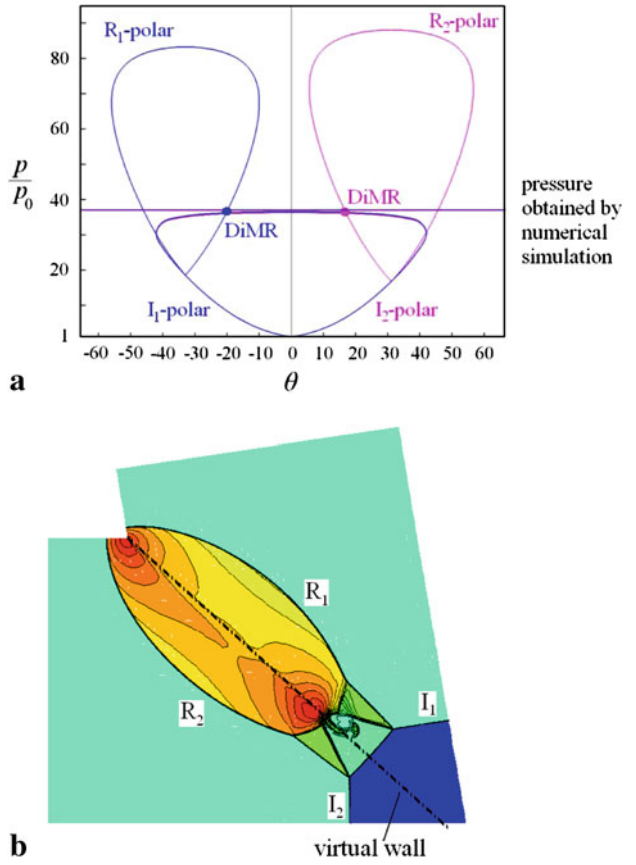

Fig. 9 The asymmetric nonstationary shock reflection of $M_{S1} = 4.0$, $M_{S2} = 3.8$ and $\theta_0 = 100°$: **a** shock polar combination; and **b** numerical result

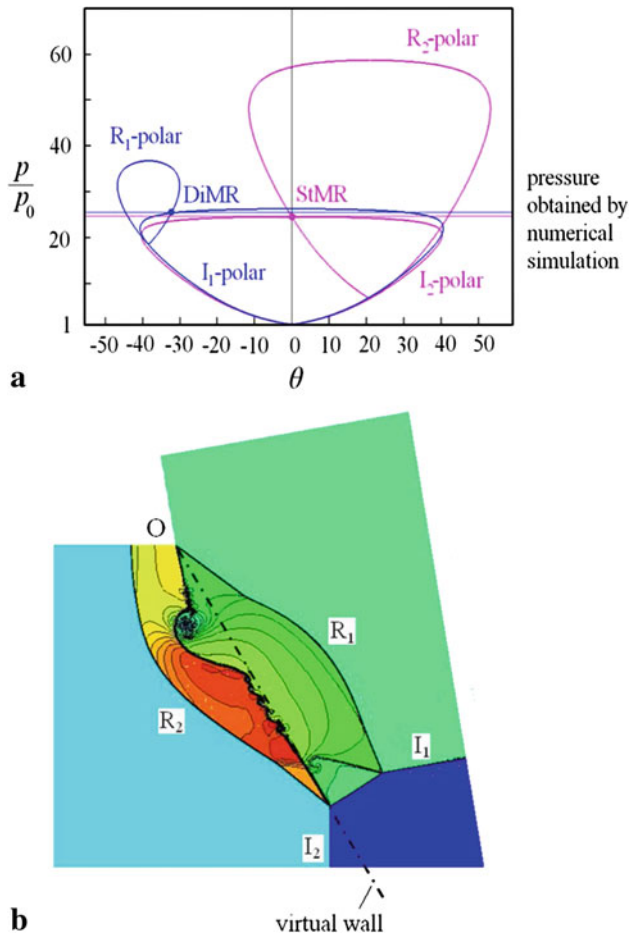

Fig. 10 The asymmetric nonstationary shock reflection of $M_{S1} = 4.0$, $M_{S2} = 2.42$ and $\theta_0 = 100°$: **a** shock polar combination; and **b** numerical result

possible. Furthermore, the intersection of the R_1-polar and the left-hand branch of the I_1-polar, together with the intersection of the R_2-polar with the right-hand branch of the I_2-polar, indicate that two DiMRs are involved in this oMR wave configuration. It should be mentioned here again that since the oncoming flow Mach numbers after the Galilean transformations depend partly on the triple point trajectory angles on each side of the virtual wall, they are thus different and hence the incident shock polar curves (I_1- and I_2-polars) are not identical either. Figure 9b shows the numerical result of this reflection. It is clear that two DMRs occur in the flowfield. The virtual wall surface, which is derived by the shock dynamic analysis, is located between the two DMRs and perpendicular to the Mach stem. In addition, the pressure ratios behind the Mach stem, which are obtained by the numerical simulation, agree well with those from the shock polar combination.

Figure 10a is the shock polar combination for the reflection of incident shock waves $M_{S1} = 4.0$, $M_{S2} = 2.42$ and the intersecting angle $\theta_0 = 100°$. In this situation, the R_1- and R_2-polars still do not intersect each other. However, unlike the above case, here the intersection point of R_2- and I_2-polars is located exactly at the middle line, which suggests that a StMR would appear on I_2 side. This kind of reflection combination is schematically illustrated in Fig. 6b. Note that the pressure ratios, which are denoted by the ordinates of the intersection points, are not exactly equal, yet they do not differ considerably in quantity (only about 3.5 % as shown in Fig. 10a) and hence can be easily matched in the flowfield. The numerical result of this asymmetric reflection is shown in Fig. 10b, in which a StMR and a TMR appear on each side, respectively. It can be seen that the triple point of the reflection on I_2 side lies on the virtual wall surface and travels along it. This is because that when I_1 meets I_2 at wedge apex O at the start stage of this reflection, the Mach stem length is exactly zero, while a StMR is a reflection in which the Mach stem length is a constant, thus the triple point on I_2 side would always be located on the virtual wall surface to maintain the Mach stem length as a constant of zero.

Figure 11a presents the shock polar combination for $M_{S1} = 2.0$, $M_{S2} = 1.4$ and $\theta_0 = 100°$, which corresponds to the reflection type shown in Fig. 6c. In this reflection,

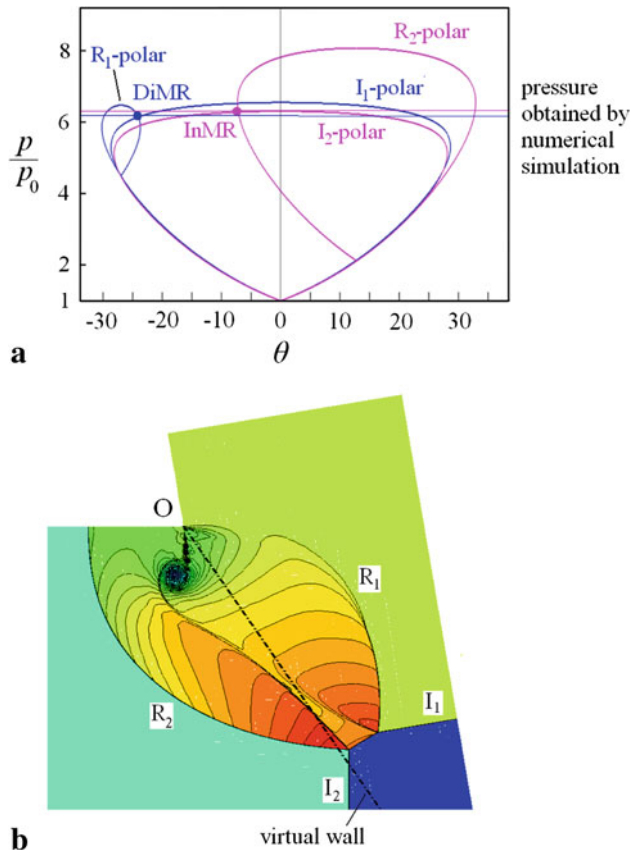

Fig. 11 The asymmetric nonstationary shock reflection of $M_{S1} = 2.0$, $M_{S2} = 1.4$ and $\theta_0 = 100°$: **a** shock polar combination; and **b** numerical result

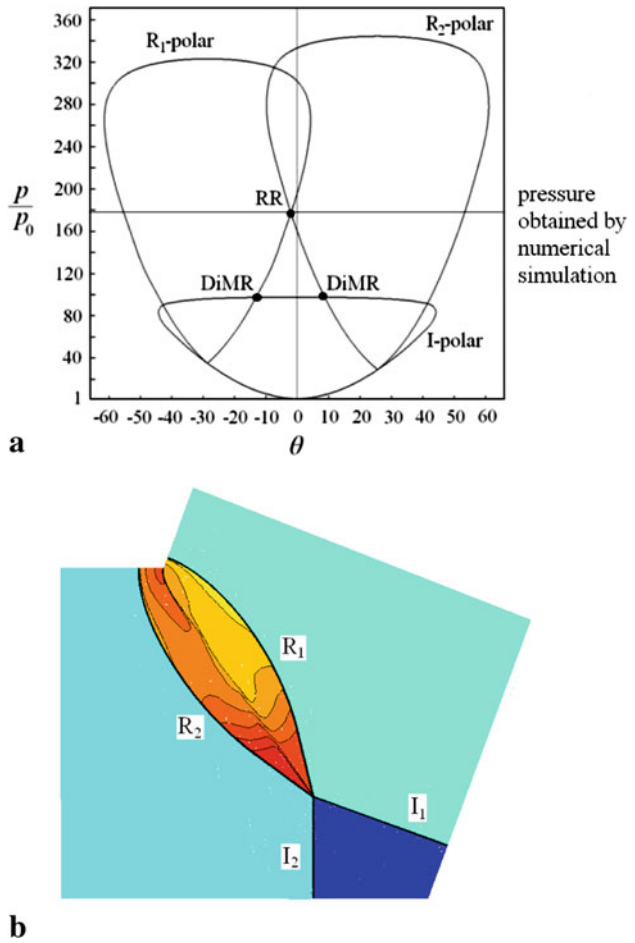

Fig. 12 The asymmetric nonstationary shock reflection of $M_{S1} = 5.5$, $M_{S2} = 5.0$ and $\theta_0 = 70°$: **a** shock polar combination; and **b** numerical result

the R_1- and R_2-polars intersect the left-hand branches of the I_1- and I_2-polars, respectively, which implies that an oMR wave configuration consisting of a DiMR and an InMR would be obtained. Same as the above case, although the pressure ratios on each side are not completely equal, it could be easily matched in the flowfield for the pressure difference is quite small (only about 2.5 %). Figure 11b shows the numerical result of the reflection, in which a SMR and an InMR appear on each side, respectively. It can be seen that the virtual wall surface in this case does not lie between the two reflections. Note again that the Mach stem length is zero when the incident shock wave I_1 encounters I_2 at the wedge apex O, which indicates that the triple point of the InMR also collides with the virtual wall at this moment. It is known that for a typical InMR, if the triple point collides with the wedge wall, the InMR would terminate and turn into a transitioned regular reflection (TRR) [26]; however, in the present asymmetric reflection, the virtual wall surface is not a real, non-penetrated wall, thus the triple point could pass through it and then continue travelling along the triple point trajectory. For this reason, the virtual wall has no intersection with the Mach stem, but still be perpendicular to it.

The shock polar combination for $M_{S1} = 5.5$, $M_{S2} = 5.0$ and $\theta_0 = 70°$ is shown in Fig. 12a, from which it is obvious that the two reflected shock wave polar curves intersect each other, in addition to the intersections of the R_1- and R_2-polars with the I-polar. Consequently, it is suggested that there are two theoretically possible solutions: the oRR and oMR (DiMR+DiMR) wave configurations. In this situation, the reflection lies in the so-called dual solution domain. Figure 12b presents the numerical result of this reflection. An oRR wave configuration, which is complemented by a slipstream, occurs in the flowfield. The pressure ratio behind the reflected shock waves, which is obtained from the numerical result, is concordant with that from the shock polar combination, as shown in Fig. 12a.

When $M_{S1} = 4.0$, $M_{S2} = 1.5$ and $\theta_0 = 70°$, the asymmetric reflection is still in the domain of dual solution. Figure 13a shows the shock polar combination of this reflection, which is also illustrated by Fig. 6g schematically. It is suggested that both the oRR and the oMR consisting of a DiMR and an InMR are possible. Figure 13b shows the

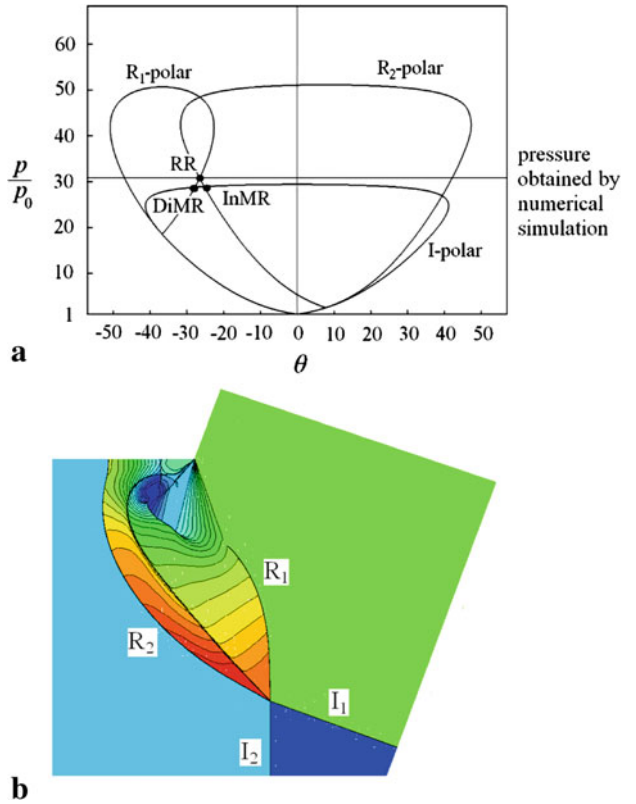

Fig. 13 The asymmetric nonstationary shock reflection of $M_{S1} = 4.0$, $M_{S2} = 1.5$ and $\theta_0 = 70°$: **a** shock polar combination; and **b** numerical result

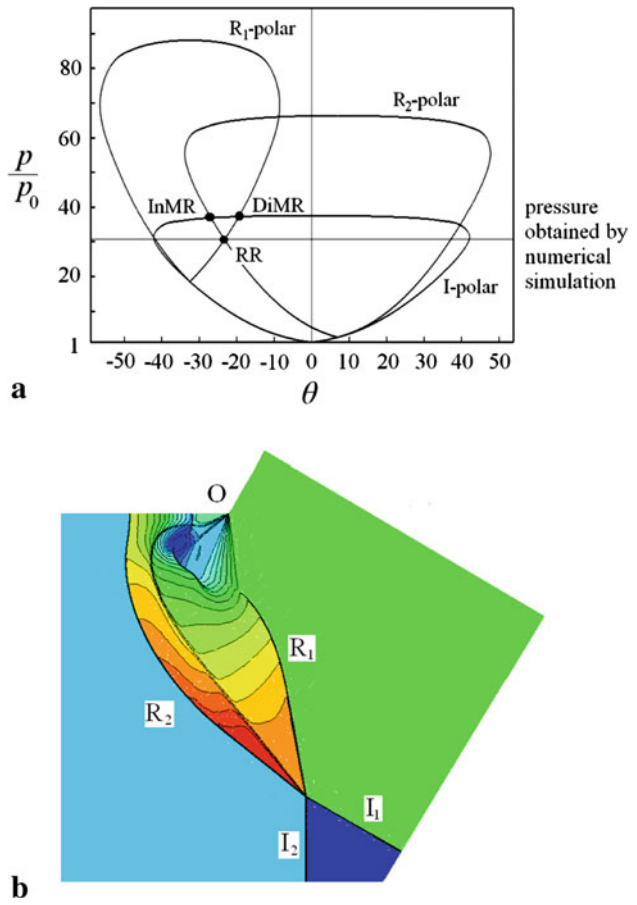

Fig. 14 The asymmetric nonstationary shock reflection of $M_{S1} = 4.0$, $M_{S2} = 1.5$ and $\theta_0 = 60°$: **a** shock polar combination; and **b** numerical result

numerical result of this reflection and once again an oRR wave configuration appears in the flowfield. Consequently, it could be deduced that the oRR, instead of the oMR wave configuration, would always occur in the dual solution domain for the asymmetric nonstationary shock reflection. This conclusion comes as no surprise because the shock reflection in pseudo-steady flows, which could also be regarded as the symmetric nonstationary shock reflection, just agrees with the detachment criterion.

Figure 14a presents shock polar combination for the asymmetric reflection of $M_{S1} = 4.0$, $M_{S2} = 1.5$ and $\theta_0 = 60°$, which corresponds to the reflection type schematically illustrated by Fig. 6i. In this reflection, although the R_1- and R_2-polars intersect the I-polar, respectively, the oMR wave configuration is impossible. The reason could be specified as follow: if an oMR wave configuration which consists of an InMR and a DiMR appears in the present case, a diverging slipstream tube would be formed which indicates that the Mach stem would be shortened with time. However, when the two incident shock waves encounter each other at wedge apex O, the reflection is just established. At this moment, the Mach stem length is zero and it could not be shortened further! Consequently, the diverging slipstream tube shaped oMR wave configuration could never appear in this self-similar shock reflection. Figure 14b shows the numerical result and an oRR wave configuration is obtained, which confirms the above theoretical consideration.

4.2 Several special reflection wave configurations

Figure 15a shows the numerical result for the asymmetric reflection of $M_{S1} = 3.0$, $M_{S2} = 1.8$ and $\theta_0 = 90°$. An oMR wave configuration which consists of a TMR and an InMR occurs in the flowfield. It is observed that the InMR appeared in the present reflection is somewhat different with the one shown in Fig. 11b. In Fig. 11b, the reflected shock wave of the InMR is curved along its entire length; while in the present case, the reflected shock wave has a straight portion which extends from the triple point to a kink, namely K. Behind the kink K the reflected shock wave is curved along its entire length. This wave configuration is analogous to the TMR wave configuration which is one of the categories of the DiMR. Figure 15b shows the numerical result for the asymmetric reflection of $M_{S1} = 5.0$, $M_{S2} = 2.65$ and

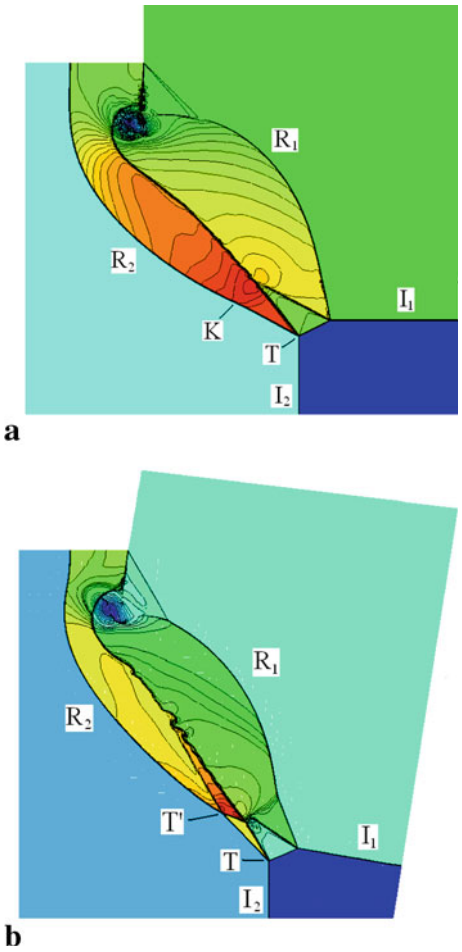

Fig. 15 The special types of inverse-Mach reflections: **a** the transitional-Mach reflection shape; and **b** the double-Mach reflection shape

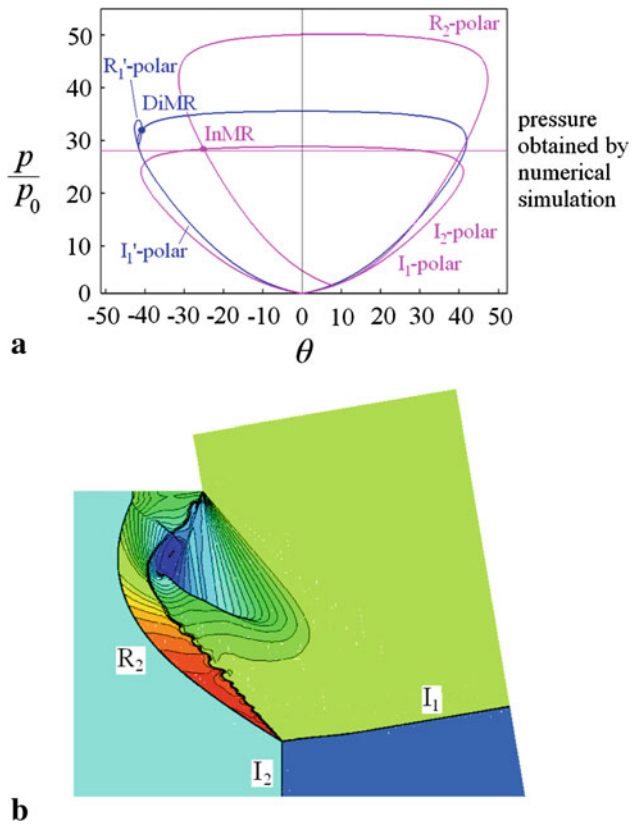

Fig. 16 The asymmetric nonstationary shock reflection of $M_{S1} = 5.0$, $M_{S2} = 1.5$ and $\theta_0 = 100°$: **a** shock polar combination; and **b** numerical result

$\theta_0 = 80°$, in which a DMR and an InMR are obtained. It is clear that the second Mach stem and the second slipstream are formed in this InMR wave configuration, which is similar to the structures formed in a DMR. Hence, the wave configurations presented in Fig. 15a,b may be regarded as the inverse-transitional-Mach reflection (InTMR) and inverse-double-Mach reflection (InDMR), respectively, which so far have never been observed in both computations and experiments. The typical InMR presented in Fig. 11b, of which the wave configuration is analogous to a SMR, could be referred to as the inverse-single-Mach reflection (InSMR). Furthermore, the transition criteria between InSMR-InTMR and InTMR-InDMR may be deduced as $M_2^T = 1$ and $M_2^{T'} = 1 + \varepsilon$ (where $\varepsilon \to 0$), which are similar to those in the pseudo-steady reflection [26]. However, the further detailed study is needed in the future to confirm the inference. In addition, since the InMR has some special configurations, it is reasonable to suppose that the TMR- and DMR-shaped StMRs, which are never recorded in the past either, would also exist in the asymmetric reflection.

Figure 16a is the shock polar combination for $M_{S1} = 5.0$, $M_{S2} = 1.5$ and $\theta_0 = 100°$. By the above analytical approach, it is predicted that only the oMR wave configuration is theoretically possible. If the oMR occurs, the I_1'- and I_2-polars are the incident shock polar curves and the R_1'- and R_2-polars are the reflected shock polar curves. It is seen that an InMR and a DiMR would appear in theory. However, note that the pressure ratios obtained from the InMR and DiMR differ considerably in quantity (about 14 % as shown in Fig. 16a), which could not be matched by the flowfield of the reflection on each side. This great pressure gap hence makes the oMR wave configuration impossible and a new configuration would appear. In the pseudo-steady shock reflection, if the flow behind the incident shock wave is subsonic with respect to the reflection point R (shown in Fig. 17a as $M_1^R < 1$), a reflected shock wave seems to be unnecessary since the subsonic flow is able to continuously turn to negotiate the wedge surface. In reality, however, a Mach reflection is always obtained because the flow particle near the wedge surface does not "know" about the obstacle until it passes through the incident shock wave and hence it needs a reflected shock wave to negotiate a sudden new boundary condition [26]. However, in the asymmetric nonstationary

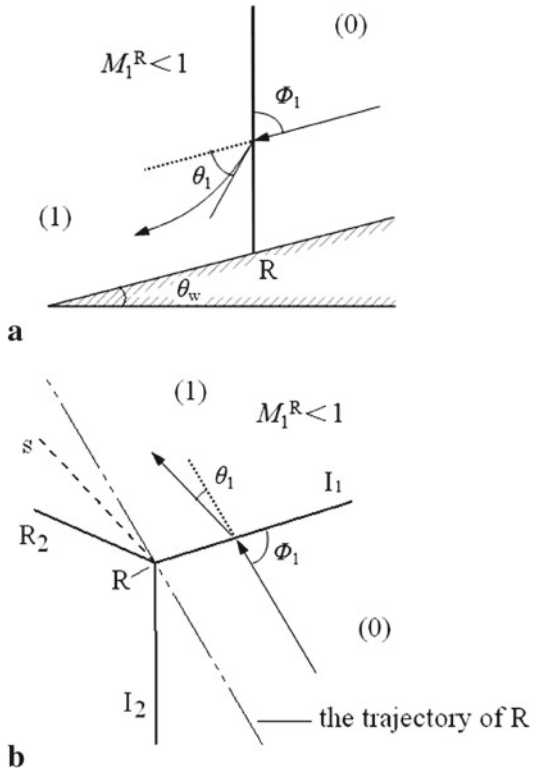

Fig. 17 The reflections in which $M_1^R < 1$: **a** shock polar combination; and **b** numerical result

shock reflection, although the situation is similar, there is an important difference: the flow passing through the incident shock wave I_1 should negotiate to the slipstream instead of the trajectory of the reflection point R (which means the wedge wall in Fig. 17a). If the left side reflection is an InMR, the slipstream direction is much easier to be negotiated than the trajectory of R (as shown in Fig. 17b), which makes the reflected shock wave on the right side unnecessary. Consequently, the InMR triggers the incident shock wave I_1 to act as a strong, non-reflection oblique shock wave. In this situation, as shown in Fig. 16a, the incident shock wave curves I_1- and I_2-polars are identical and the flow state behind the incident shock wave I_1 is denoted by the point located on the strong portion of the I_1-polar, which also denotes the state behind the reflected shock wave R_2. Thus, the pressure on each side could eventually be identical. Figure 16b presents the numerical result of this reflection, in which an InMR wave configuration appears on the left side yet no reflection occurs on the right side. The incident shock wave I_1 is bent up slightly to negotiate the flow passing through it to the direction parallel to the slipstream. Since no typical Mach stem is obtained in this reflection, the InMR is converted to a RR and the overall configuration could be regarded as a special oRR wave configuration. Nevertheless, it should be pointed out that this special reflection wave configuration is formed only when the two incident shock wave Mach numbers differ greatly, for which the pressure behind the Mach stem on each side could not be matched and the above-mentioned analytical approach gets invalid. In most situations of the asymmetric nonstationary shock reflections, the assumption of the virtual wall is appropriate and the shock dynamic–shock polar combined analytical approach is still available.

4.3 Domains of various types of reflections

Applying the above-mentioned approach, the domains and transition boundaries of various types of reflection wave configurations could be predicted analytically. Figure 18a–d presents the domains for the intersecting angle $\theta_0 = 100°, 90°, 80°$ and $75°$, respectively. The ordinates denote the Mach numbers of the incident shock wave I_1 and the abscissas denote the Mach numbers of I_2. The black solid lines, which are derived by the detachment criterion for asymmetric shock reflection, show the transition boundaries between the oRR and oMR wave configurations. The dashed lines present the boundary between the InMR and the DiMR, while the dot dash lines and the double dot dash lines, which are calculated from $M_2^T = 1$ and $M_2^{T'} = 1 + \varepsilon$ (where $\varepsilon \to 0$) [26], present the boundaries of SMR-TMR and TMR-DMR, respectively. It should be noted that the PTMR wave configuration, which is put forward in [26], is classified as TMR here, to avoid the analytical results too complex. The lines with blue colour denote the reflection configurations on I_1 side, e.g., a TMR wave configuration appears on I_1 side for $M_{S1} = 5.0$, $M_{S2} = 2.5$ and $\theta_0 = 100°$; the lines with red colour denote the reflection configurations on I_2 side, e.g., an InMR wave configuration appears on I_2 side for $M_{S1} = 5.0$, $M_{S2} = 2.5$ and $\theta_0 = 100°$. Thus, it could be known that an oMR wave configuration which consists of a TMR and an InMR is formed in the case of $M_{S1} = 5.0$, $M_{S2} = 2.5$ and $\theta_0 = 100°$. Consequently, the overall reflection wave configuration, together with the reflection types on both sides of the virtual wall, could be obtained from Fig. 18 for every combination of M_{S1} and M_{S2}. It is shown that the oRR domain enlarges with the increase of θ_0, which is due to the fact that an oRR is more likely to form if the angle between the two shock waves is relatively small. The numerical results, which are plotted by various symbols and marked with the reflection types on both sides for the oMR cases, show good agreement with the analytical domains.

4.4 The effect of mis-synchronization

It should be noted that two nonstationary shock waves meeting at the wedge apex at exactly the same time, as discussed above, is just an extremely ideal condition, while the asymmetric shock wave reflection with mis-synchronization is more likely to occur in reality. Thus, it is necessary here to discuss the effect of mis-synchronization in this asymmetric

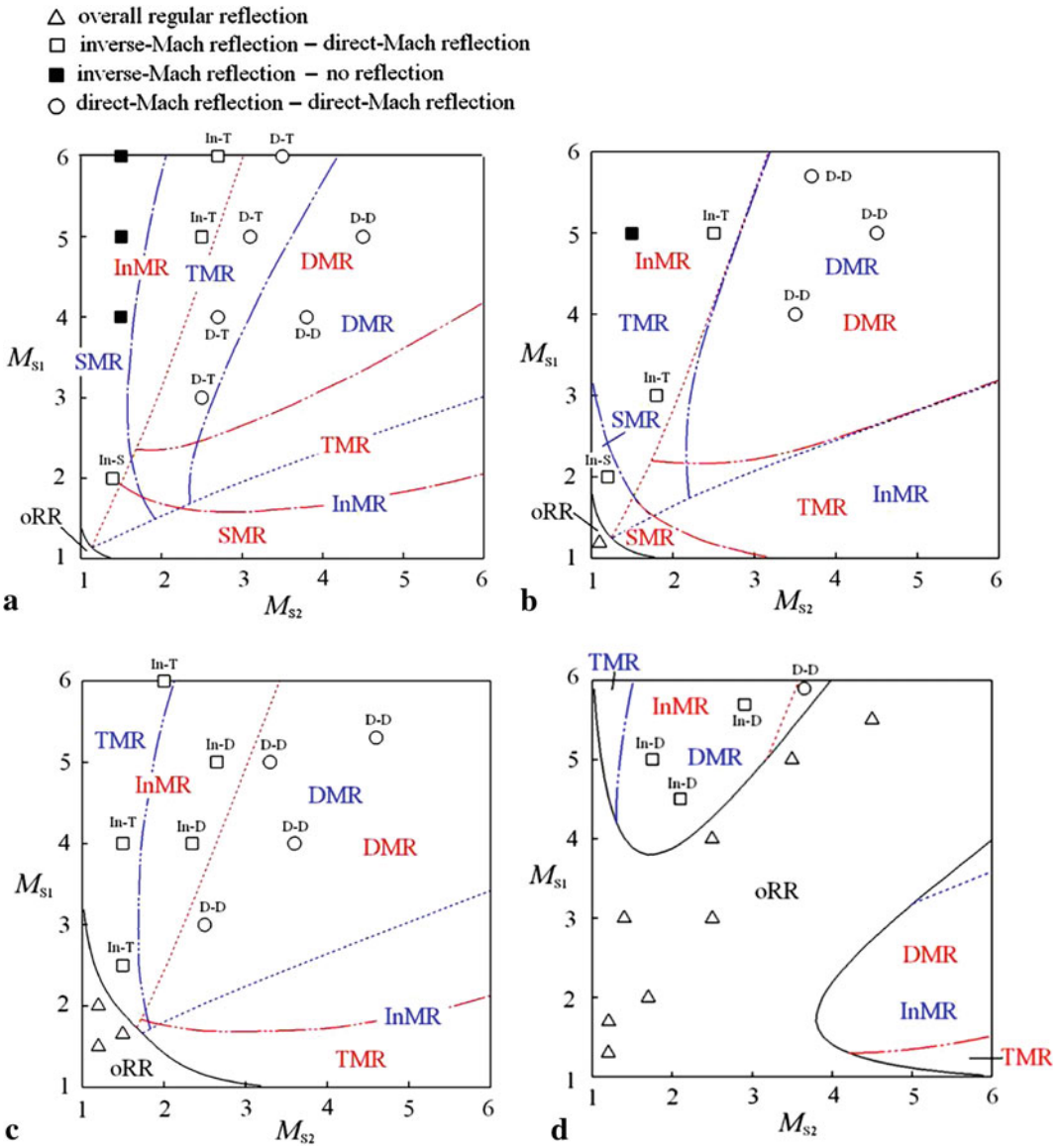

Fig. 18 The domains of various types of reflection wave configurations (In-InMR, S-SMR, T-TMR, D-DMR): **a** $\theta_0 = 100°$; **b** $\theta_0 = 90°$; **c** $\theta_0 = 80°$; **d** $\theta_0 = 75°$

shock wave reflection. In the mis-synchronized cases, the incident shock waves arrive at the apex at different moments, as illustrated in Fig. 19a, so a mis-synchronization distance δx, which indicates the distance between the late wave I_2 and the apex O at the moment when the early wave I_1 reaches the apex O, would exist. Consequently, the early wave I_1 would diffract around the wedge and a vortex would be formed, and then the late wave I_2 would interact with both the diffracted shock wave and the vortex. At the early stage of the interaction, the intersecting angle between the late wave I_2 and the diffract shock wave is quite small, so an oRR configuration would be obtained. However, since the intersecting angle increases with time, the transition from an oRR to an oMR might occur in some later stage. Figure 19b illustrates the flowfield structures at the exact moment of the transition. If this transition occurs when the late wave I_2 still interacts with the diffracted shock wave, the triple point trajectories of the oMR would not be straight, because this oMR configuration is formed by an interaction between a planar and a curved shock wave. Later on, when the late wave I_2 starts to interact with the early wave I_1 directly, the triple point trajectories would become straight, and the self-similar reflection configuration would eventually be established. The triple point trajectories are illustrated as dot dash lines in Fig. 19b. The dash lines, however, indicate the extension lines of the straight parts of the triple point trajectories, and they finally meet at the point B, which could be regarded as the origin of the subsequent self-similar oMR configuration.

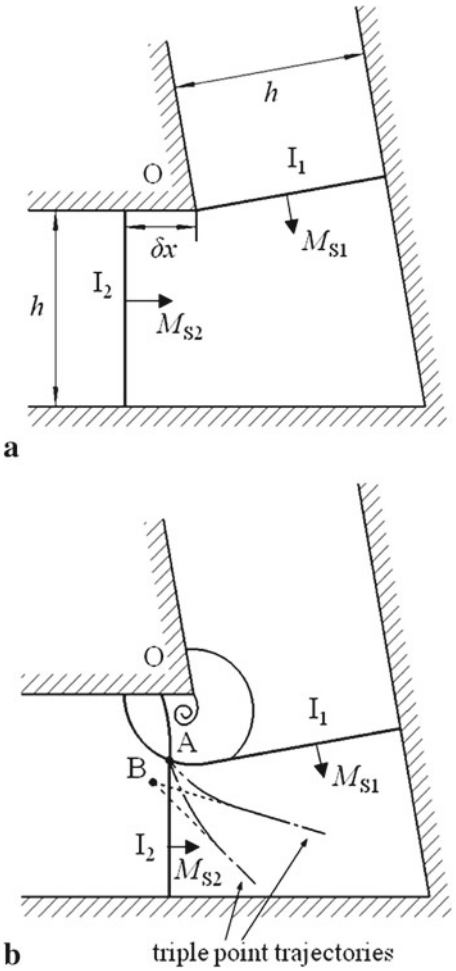

Fig. 19 The illustrations of asymmetric nonstationary shock reflection with a mis-synchronization distance: **a** the initial moment; and **b** the moment of the transition from an oRR to an oMR

Figure 20a–c shows asymmetric nonstationary shock reflections for $M_{S1} = 4.0$, $M_{S2} = 2.42$ and $\theta_0 = 100°$, with mis-synchronization distances δx=1.5, 3.0 and 4.5 mm, respectively. These mis-synchronization distances are equivalent to 3, 6 and 9 % of the shock tube width h, respectively, and the results in these figures are the flowfields at the moments when the late shock waves I_2 arrive at nearly the same x-direction locations. It can be seen that although different wave and vortex structures are formed around the apex O for different mis-synchronization distances δx, almost the same asymmetric shock wave reflection configurations are obtained. That is, a DiMR appears on I_1 side, and a StMR, in which the triple point travels along the virtual wall, appears on I_2 side. This configuration is also the same as the one in the ideal condition, i.e., the synchronized reflection, as shown in Fig. 10b. Compared to the synchronized case, in which the virtual wall originates at the apex O, in the mis-synchronized case, however, the virtual wall originates at the point B instead. This is because the point B, as discussed above and shown in Fig. 19b, could be regarded as the origin of the self-similar oMR configuration. From these results, It could also be found that the distance from the origin B to the apex O has a linear relation with δx, that is, larger δx would lead to a larger distance between B and O. Figure 20d shows a different mis-synchronized case, in which the shock wave I_1, instead of I_2, is the late wave, and the distance between I_1 and the apex O is $\delta y = 3.0$ mm at the moment when the early wave I_2 arrives at apex O. In this situation, the shock wave I_2 would diffract around the apex O at the early stage, thus the origin B is located on I_1 side. Compared to the $\delta x = 3.0$ case shown in Fig. 20b, here the distance from B to O is much shorter, and this is because I_2 is the relatively weak wave and thus would interact with I_1 soon after passing the apex. It can be seen that almost the same oMR configuration, which consists of a StMR and a DiMR, is also formed in this situation. Consequently, no matter δx or δy exists, the same asymmetric shock wave reflection configuration as the ideal synchronized case would appear, although some different flowfield structures appear around the wedge apex. Thus, the above-mentioned shock dynamic–shock polar combined analytical method could also be performed in the synchronized cases to predict the reflection configuration.

It should also be mentioned that the reflection flowfields for different mis-synchronization distances on the same side (e.g., the ones shown in Fig. 20a–c), including the wave and vortex structures around the apex, are in fact the flowfields of a unique case but at different stages. For example, for an asymmetric reflection in which the mis-synchronization distance is $2\delta x$ and the width of the tube is $2h$, the flowfield configuration is similar to the one in Fig. 19a in which the distance is δx and the width is h, only with linear increases of space and time scales. Consequently, there are only three essentially different flowfield configurations for a combination of the given incident shock Mach numbers and intersecting angle: the ideal synchronized one, the one with a mis-synchronization distance on I_1 side and the one with a mis-synchronization distance on I_2 side. Moreover, it should be noted that the latter two would gradually approach the ideal synchronized one with time, because the effect of δx or δy would get smaller with the increase in size of the asymmetric reflection configuration.

5 Conclusions

The reflections of asymmetric nonstationary shock waves are analytically and numerically investigated in this paper. The shock dynamic and shock polar approaches are combined to predict the wave configurations of the reflections. Numerical simulations are performed for validation and agree well with the analytical predictions. The results obtained in the paper could be summarized as follows:

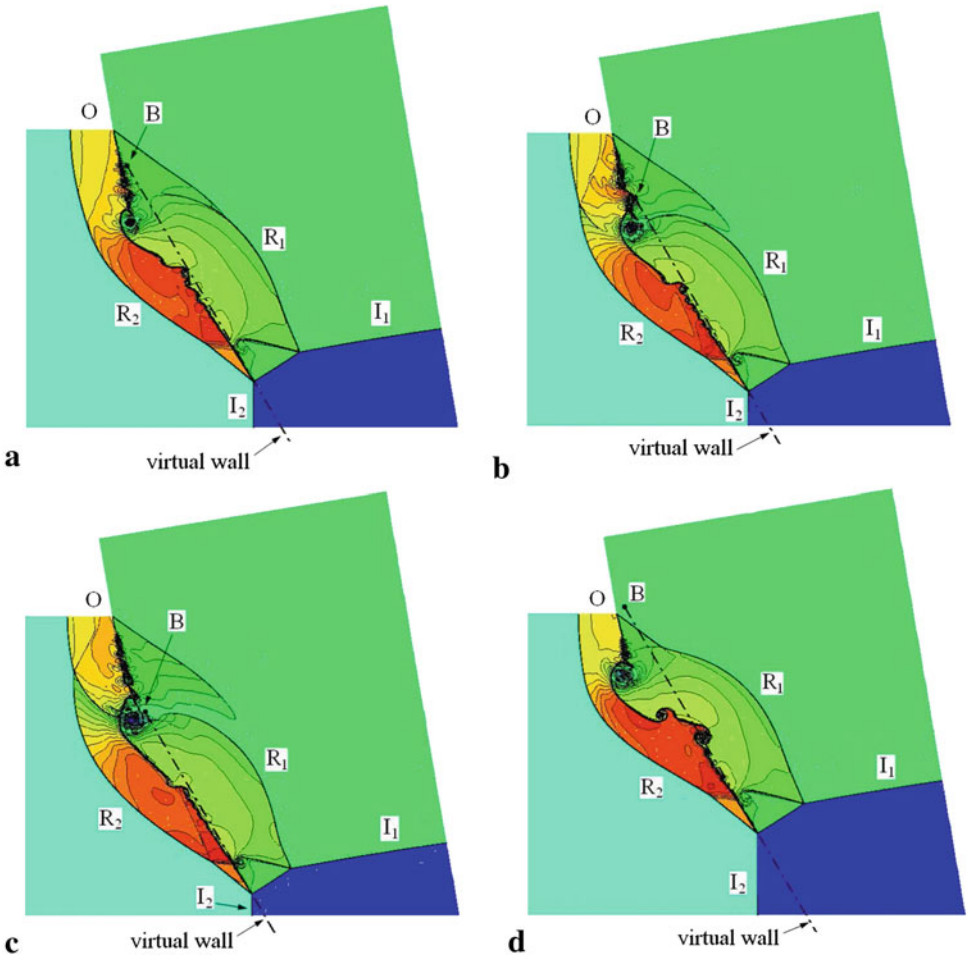

Fig. 20 The asymmetric nonstationary shock reflections of $M_{S1} = 4.0$, $M_{S2} = 2.42$ and $\theta_0 = 100°$ with different mis-synchronization distances: **a** $\delta x = 1.5$ mm; **b** $\delta x = 3.0$ mm; **c** $\delta x = 4.5$ mm; **d** $\delta y = 3.0$ mm

1. The overall Mach and regular reflection wave configurations are obtained by both analyses and computations. It is shown that the inverse- and stationary-Mach reflections, which are so far only observed in unsteady or asymmetric steady shock wave reflections, are also found to exist in the asymmetric nonstationary shock wave reflections.
2. It is figured that only overall regular reflection could appear in the dual solution domain, which is the same as the behavior of the shock wave reflection in pseudo-steady flows.
3. Two special types of inverse-Mach reflections, which are analogous to the transition-Mach reflection and double-Mach reflection, are observed in numerical results. A special type of overall regular reflection, in which one of the incident shock waves is not reflected, is also found. The reason for the existence of the reflection configuration is theoretically illustrated.
4. The domains and transition boundaries of various types of reflections are predicted analytically for the intersecting angle $\theta_0 = 100°, 90°, 80°$ and $75°$. The overall wave configuration, with the reflection types on both sides, could be obtained from the figures.
5. For the asymmetric reflection with a mis-synchronization distance at the initial moment, the same reflection configuration as the corresponding synchronized one would be obtained, and thus could also be analytically predicted by the shock dynamic–shock polar combined method.

Acknowledgments This work is supported by the National Natural Science Foundation of China (90916028,11142006).

References

1. Mach, E.: *Über* den Verlauf von Funkenwellen in der Ebene undim Raume. Sitzungsbr Akad Wien **78**, 819–838 (1878)
2. von Neumann, J.: Oblique reflection of shocks, Explos Res Rept 12, Navy Dept Bureau of ordinance, Washington, DC, USA (1943)
3. von Neumann, J.: Refraction, intersection and reflection of shock waves, NAVORD Rep 203-45, Navy Dept Bureau of ordinance, Washington, DC, USA (1943)
4. Smith, L.G.: Photographic investigation of the reflection of plane shocks in air, OSRD Rep 6271, Off Sci Res Dev, Washington, DC, USA (1945)
5. White, D.R.: An experimental survey of the Mach reflection of shock waves. Ph.D. thesis, Princeton University (1951)

6. Henderson, L.F., Lozzi, A.: Experiments on transition of Mach reflection. J. Fluid Mech. **68**, 139–155 (1975)
7. Hornung, H.G., Taylor, J.R.: Transition from regular to Mach reflection of shock waves. Part 1. The effect of viscosity on the pseudo-steady case. J. Fluid Mech. **123**, 145–153 (1982)
8. Mirels, H.: Mach reflection flow fields associated with strong waves. AIAA J. **23**, 522–529 (1985)
9. Takayama, K., Ben-Dor, G.: Pseudo-steady oblique shock wave reflections over water wedges. Exp. Fluids **8**, 129–136 (1989)
10. Colella, P., Henderson, L.F.: The von-Neumann paradox for the diffraction of weak shock waves. J. Fluid Mech. **213**, 71–94 (1990)
11. Ben-Dor, G., Glass, I.: Domains and boundaries of non-stationary oblique shock-wave reflections. 1. Diatomic gas. J. Fluid Mech. **92**(3), 459–496 (1979)
12. Ben-Dor, G., Glass, I.: Domains and boundaries of non-stationary oblique shock-wave reflections. 2. Monatomic gas. J. Fluid Mech. **96**(4), 735–756 (1980)
13. Ben-Dor, G.: Analytical solution of double-Mach reflection. AIAA J. **18**, 1036–1043 (1980)
14. Ben-Dor, G.: A reconsideration of the three-shock theory for a pseudo-steady Mach reflection. J. Fluid Mech. **181**, 467–484 (1987)
15. Ben-Dor, G., Vasilev, E.I., Henderson, L.F., Elperin, T.: The wall-jetting effect in Mach reflection: a numerical investigation. In: Proceedings of the 24th International Symposium on Shock Waves, Beijing, China, pp 461–466 (2004)
16. Ben-Dor, G.: A state-of-the-knowledge review on pseudo-steady shock-wave reflections and their transition criteria. Shock Waves **15**, 277–294 (2006)
17. Chpoun, A., Lengrand, J.C.: Confermation exprimentale d'un phnomne d'hystrsis lors de l'interaction de deux chocs obliques de familles diffrentes. C R Acad. Sci. Paris **304**, 1 (1997)
18. Li, H., Chpoun, A., Ben-Dor, G.: Analytical and experimental investigations of the reflection of asymmetric shock waves in steady flows. J. Fluid Mech. **390**, 25–43 (1999)
19. Hu, Z.M., Myong, R.S., Kim, M.S., Cho, T.H.: Downstream flow condition effects on the RRMR transition of asymmetric shock waves in steady flows. J. Fluid Mech. **620**, 43–62 (2009)
20. Barbosa, F., Skews, B.: Experimental confirmation of the von Neumann theory of shock wave reflection transition. J. Fluid Mech. **472**, 263–282 (2002)
21. Barbosa, F., Skews, B.: Shock wave interaction with a spiral vortex. Phys. Fluids **13**, 3049–3060 (2001)
22. Xie, P., Han, Z.Y., Takayama, K.: A study of the interaction between two triple points. Shock Waves **14**(1), 29–36 (2005)
23. Toro, E.: Riemann solvers and numerical methods for fluid dynamics: a practical introduction. Springer, Berlin (1997)
24. Li, H.H.: Experimental and numerical study on unsteady complex flow and wave interaction. PhD Thesis. University of Science and Technology of China, Hefei (2005)
25. Sun, M.: Numerical and experimental studies of shock wave interaction with bodies. PhD Thesis, Tohoku University, Sendai (1998)
26. Ben-Dor, G.: Shock wave reflection phenomena. 2nd edn. Springer, Berlin (2007)